

Review

An Overview of the Design and Optimized Operation of Vanadium Redox Flow Batteries for Durations in the Range of 4–24 Hours

Vilayanur V. Viswanathan , Alasdair J. Crawford, Edwin C. Thomsen, Nimat Shamim, Guosheng Li, Qian Huang and David M. Reed

Battery Materials & System Group, Pacific Northwest National Laboratory, Richland, WA 99352, USA

* Correspondence: vilayanur.viswanathan@pnnl.gov; Tel.: +1-509-372-4745

Abstract: An extensive review of modeling approaches used to simulate vanadium redox flow battery (VRFB) performance is conducted in this study. Material development is reviewed, and opportunities for additional development identified. Various crossover mechanisms for the vanadium species are reviewed, and their effects on its state of charge and its state of health assessed. A stack design focusing on flow fields and an electrode design tailored to various flow fields are reviewed. An operational strategy that takes these parameters into account is reviewed for various operating envelopes, chosen based on end user preference in terms of minimizing capital cost or operation and maintenance cost. This work provides a framework for the design and operation of a VRFB for various grid services.

Keywords: vanadium redox flow battery (VRFB); stack design; crossover; state of charge; modeling approach; materials development; flow field



Citation: Viswanathan, V.V.; Crawford, A.J.; Thomsen, E.C.; Shamim, N.; Li, G.; Huang, Q.; Reed, D.M. An Overview of the Design and Optimized Operation of Vanadium Redox Flow Batteries for Durations in the Range of 4–24 Hours. *Batteries* **2023**, *9*, 221. <https://doi.org/10.3390/batteries9040221>

Academic Editor: George Zheng Chen

Received: 17 February 2023

Revised: 1 April 2023

Accepted: 3 April 2023

Published: 6 April 2023



Copyright: © 2023 by the authors. Licensee MDPI, Basel, Switzerland. This article is an open access article distributed under the terms and conditions of the Creative Commons Attribution (CC BY) license (<https://creativecommons.org/licenses/by/4.0/>).

1. Introduction

With increased renewable penetration in the power grid, there is a need for batteries with the capability for long-duration energy storage (LDES) applications in the range of 10–24 h [1]. This is due to the intermittent nature of renewable sources, such as solar and wind, which require the development of storage technologies that can store this intermittent energy and deliver the stored energy as needed [2]. Redox flow batteries are ideal for durations greater than 6 h, where the stack cost can be distributed over a larger energy base. To be cost-effective, reversible and irreversible capacity losses need to be minimized and the utilization of electrolyte maximized. This paper addresses material development for all-vanadium redox flow batteries (VRFBs) in the areas of electrodes, bipolar plates and electrolyte; examines, in detail, the crossover mechanisms and associated mitigation approaches; reviews the approaches to measuring state of charge (SOC) and state of health (SOH); reviews electrode design, flow field design and their interactions; and discusses the various operational strategies that optimize the chosen objective function, e.g., minimizing capital cost, operation and maintenance costs and levelized cost, which are dependent on specific regional requirements and the end user business model.

The authors of [3] provided an overview of redox flow battery reactions (during charge, discharge, self-discharge and side reactions during overcharge), reaction mechanisms, electrode kinetics, performance as a function of electrolyte flow rate, and the theoretical estimation of limiting current densities as a function of flow rate and flow pattern. Another excellent review of critical VRFB issues included VRFB electrochemistry, overpotentials, a review of the core components (electrodes, electrolyte, membranes, bipolar plates), various modeling approaches, flow field design, operational strategies, stack design, challenges and development trends [4].

This paper focuses on all-vanadium redox flow batteries, since they are the most developed of the redox flow battery technologies. One of the advantages of an all-vanadium redox flow battery is that capacity decay due to the crossover of vanadium species can be restored using various balancing methods. The performance of a 15-cell stack using mixed-acid electrolyte was determined by Reed et al. [5] under different operating conditions—flow-through design, interdigitated design and varying flow rate. The interdigitated design enabled the use of a 3X higher flow rate than a conventional flow path through the electrodes for a fixed pressure drop, resulting in an improvement in stack energy efficiency from 66% to 70% at a current density of 320 mA/cm^2 , with a more modest increase from 73% to 76% at 240 mA/cm^2 . The effects of operating temperature at various current densities and flow rates were also explored for the interdigitated design to obtain a suitable operating envelope. These data were used to update a previously developed cost-performance model [6] to perform techno-economic analysis on an all-vanadium redox flow battery after validating model performance prediction across all current densities and flow rates [7]. The validated model was also used to predict the performance of Fe-Cr and F-V redox flow batteries to enable cost comparison. The all-vanadium chemistry was found to be the most cost-effective at USD 300/kWh, followed by Fe-Cr at USD 400/kWh and Fe-V at USD 600/kWh.

An analytical performance model was developed and validated using data for zinc-based and S/Br₂ single cells, and a 15-cell all-vanadium stack [8]. Cost comparison was performed versus all-vanadium batteries for a 1 MW, 8 MWh system, with the zinc-based chemistry showing lower cost across the 20–150 mA/cm² current density range, building on the approach described by Viswanathan et al. [6]. Similar analysis needs to be performed on the levelized cost of storage, as described in the Energy Storage Grand Challenge Phase 2 report [9]. Another promising flow battery chemistry is the zinc iron redox flow battery, which has potential to reach a capital cost of USD 100/kWh, though challenges such as zinc dendrite growth need to be overcome [10].

A deep dive into redox flow battery materials is beyond the scope of this article, but information is available in the literature [11]. The following section covers modeling as it pertains to implementation in the battery management system (BMS), material development, tools for state of charge (SOC) and state of health (SOH) estimation, crossover mechanisms, BMS approaches, stack design and environmental impact. Where appropriate, gaps that need to be addressed are highlighted.

Figure 1 is a schematic of a vanadium redox flow battery (only one cell is shown) with balance of plant, while Figure 2 shows individual components within a cell with various flow fields in the bipolar plate. Note that VO²⁺ and VO₂⁺ correspond to V⁺⁴ and V⁺⁵, respectively.

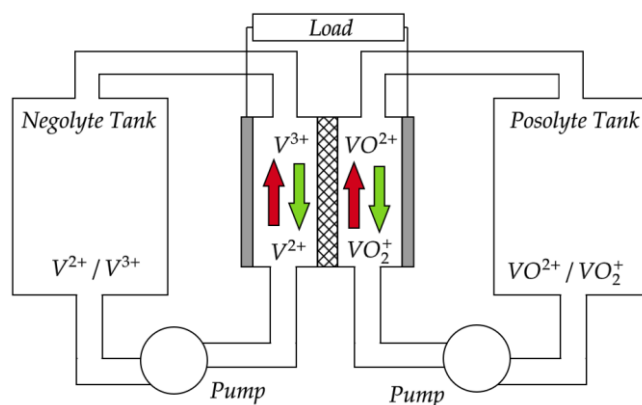


Figure 1. Schematic of vanadium redox flow battery (green is charge and red is discharge).

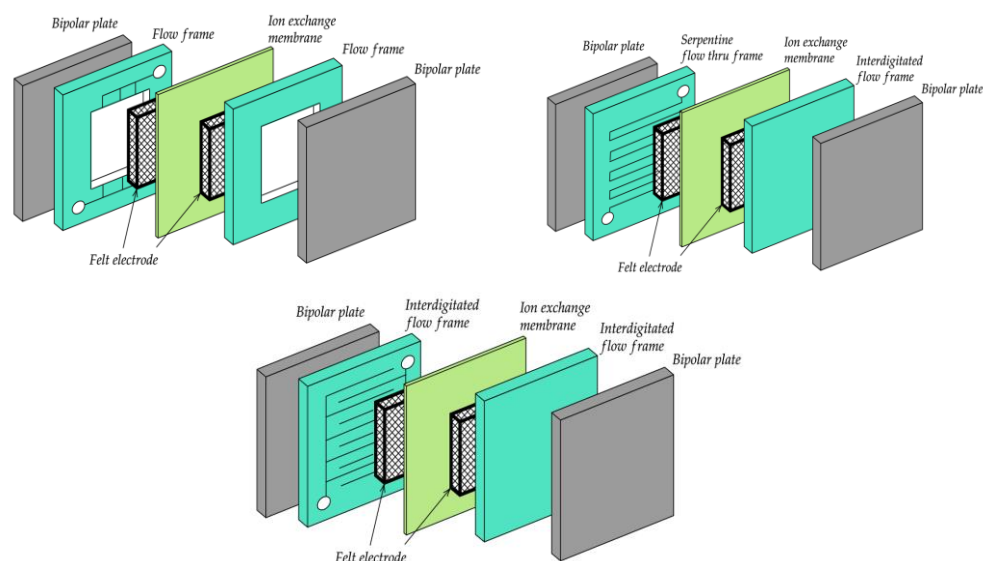


Figure 2. Individual components within a cell with various flow fields in the bipolar plate flow-through (**top left**), interdigitated (**top right**), serpentine flow-by (**bottom**).

While this review focuses on all-vanadium redox flow batteries, other approaches to increasing energy density for LDES applications include slurry flow batteries [12–14] and using redox mediators [15,16]. The high viscosity of slurries results in a large pressure drop, while the presence of conductive fillers, such as carbon black, increase shunt current losses. To circumvent this, slurries of a LiCoO_2 positive active material were prepared without conductive fillers [14]. While they worked in principle, the active material utilization was too low; hence, more development work needs to be conducted.

To remove the limitations associated with slurry systems while retaining their high energy density, the electroactive species was stored at a cooler temperature in tanks, where it resided in a saturated condition, with the solids on the tank bottom separated from the dissolved active species by a separator. The liquid was pumped into the stack via a heat exchanger, where it was heated to a higher temperature such that it entered and exited the stack with the electroactive reactants and products fully dissolved [17]. By adjusting the solid-to-liquid ratio in the tank, the energy density is adjusted as desired for the LDES application. More work needs to be conducted to increase the precipitation rate in the tank such that it is not a limiting factor.

The limitations of slurry-based systems and two-phase systems, as described above, are addressed using a redox mediator in a dissolved state that is oxidized or reduced at the stack electrodes, and exchanges electrons with the storage material that exists in a solid phase in the tank; this produces energy density an order of magnitude higher than that of conventional redox flow batteries [15,16]. Several redox materials have been identified that match the potential range of the solid storage medium. While solid material utilization still needs to be improved, this approach opens a pathway to combine the high advantage of conventional redox flow batteries, in terms of separation of power and energy, with the high energy density of solid electroactive material.

2. Modeling

The simulation of battery operation for various stack designs, durations and operating conditions can significantly reduce upfront expenses in trial and error. Modeling can be grouped into physics-based electrochemical/thermal/fluid dynamics models versus equivalent circuit modeling, with properties considered to be distributed across the modeling space or lumped into one average value [18]. Table 6 in [19] groups references for the above approaches into models that consider properties as lumped or distributed. In their study, the interdependence of the physics-based models is described; for example, the electrochemical model results depend on the stack temperature distribution predicted by

the thermal model; the electrochemical model's outputs, such as the species concentration distribution in the stack, the operating voltage, the current and the flow rate, affect the thermal model results, while the fluid dynamics model is affected by the current and SOC-dependent flow rate. This indicates that coupling of electrochemical/thermal/fluid dynamics models is needed to reliably predict performance and degradation. Note that model validation should be performed using reliable SOC measurement techniques, which are described in detail in the SOC estimation in Section 4.1.

For BMS implementation, using a simplified or reduced form of these coupled physics-based models without loss of reliability is paramount. Another option is to develop an equivalent circuit model with input from the coupled models to adjust the circuit parameters as a function of stack design. The limitation of this approach is that it can only be used to predict initial performance, with unreliable prediction of crossover rate and stack component degradation.

Utilizing previous work on polymer electrolyte membrane fuel cells, a reduced model that kept the system geometry intact was used to decrease computation time by up to three orders of magnitude [20]. This work assumes only proton crossover, and hence, ignores capacity decay due to vanadium species transport across the membrane. Analytical models were developed and validated versus finite element models [21], thus providing scope for implementation in a BMS.

The flow battery stack was modeled as a plug flow reactor system to estimate species concentration and cell voltage along the flow path for current density in the range of 75–200 mA/cm², for a 1500 cm² cell, over a wide range of stoichiometric values of 3–9, where the stoichiometric value was a multiple of the stoichiometric flow rate [22]. At the lower end of the current density range, charging could be performed up to ~90% SOC without gas evolution, while the SOC had to be restricted to < 80% when the current density was >165 mA/cm². This indicates the importance of a charge algorithm to reduce charge power as SOC approaches 80% as a function of the maximum allowable flow rate for the system. Note that as the charge proceeds, the reactant concentration decreases, and hence, the required flow rate for fixed stoichiometry increases. The modeling also predicted electrolyte imbalance, based on the SOC difference between positive and negative electrolytes.

While hydraulic models are useful, Xu and Zhao [23] reviewed the lattice Boltzmann method to estimate flow through porous media while taking into account material wettability; they used the Monte Carlo method to generate the porous electrode geometry, with the finite volume method used to predict battery performance. The article also discussed the use of X-ray computer tomography to conduct an in-depth study of porous electrode geometry. The key here is that the Monte Carlo method can generate various porous geometries for the simulation of battery performance, while X-ray computer tomography is used to determine the structure of an existing felt electrode. This paper highlights the importance of using the Monte Carlo method and X-ray computer tomography to understand porous electrode geometry for input into hydraulic models. It can also be surmised that the validation of hydraulic models using the lattice Boltzmann model for a fixed porous electrode geometry and flow rate would enhance model reliability for future use.

Since vanadium species crossover is a key issue that needs to be better understood and addressed, the modeling of various crossover mechanisms is covered in detail in Section 4.2. Section 6 on stack design covers modeling efforts in stack sizing, flow field design and electrode design.

The path forward in the modeling landscape should focus on BMS implementation using reduced-order physics-based coupled models, or analytical models validated by reliable physics-based coupled models with simplified assumptions, such as a stack modeled as a plug flow reactor. Note that BMS implementation takes into account the electrode, the flow field design, crossover mechanisms and the effect of flow rate on performance at various SOCs to arrive at optimum operational parameters for charge and discharge. This will allow for the prediction of performance and degradation, which takes into account crossover-related reversible loss and gas ingress- or gas evolution-related irreversible loss.

3. Materials

Stack component materials are covered at various levels of detail based on opportunities for further research. Detailed specifications for tank designs are available [24], but this topic is beyond the scope of this article. The balance of plant components, such as pumps, pipes, valves, and manifolds, is not covered.

3.1. Membranes

A comprehensive review has been provided on the various types of membrane, their fabrication procedures and the test procedures to evaluate their conductivity, strength and durability [25,26]. Nafion™, which is currently the most widely used membrane in redox flow battery stacks, has good conductivity for protons and good resistance to an acid environment, but also has a non-negligible vanadium species crossover rate.

Nafion™ membranes for VRFB range in thickness from 25 microns to 180 microns; the thinner membranes are solution cast, while thicker membranes are extruded. To reduce crossover, oxides such as SiO₂ and TiO₂ are incorporated to form Nafion™ composite membranes [25]. Composites of Nafion™ with sulfonated poly ether ketone (S-PEEK), Poly Tetra Fluoro Ethylene (PTFE) and polypropylene have also been proposed to reduce crossover [25].

Sulfonated polyether ether ketone (S-PEEK) membranes, which are the leading alternative choice to Nafion™, have a lower vanadium crossover rate, with an optimum degree of sulfation, ensuring good conductivity with high durability [27]. High degrees of sulfation lead to membrane swelling in an aqueous environment, compromising durability.

While anion exchange membranes eliminate vanadium species crossover, their conductivity and durability in acidic environments are low, which has limited their use in VRFB applications. However, with the advent of long-duration energy storage (LDES) > 20 h, they may also have a role, if their durability is increased. Membrane modification to minimize crossover and its effect on electrode degradation are discussed in Section 4.3.

3.2. Electrode Development

Electrodes need to have good activity and durability and tailored porosity to ensure low pressure drops while also ensuring sufficiently high electrolyte velocity to promote fast mass transport, taking into account the flow field architecture and the maximum current density/flow rate the stack can accommodate. Electrode treatment to improve activity and durability includes thermal activation, chemical treatment with acid, electrochemical oxidation, metal and metal oxide catalyst incorporation [28,29], coating, doping, metal oxide modification [30] and carbon black coating of large-diameter electro-spun fibers with high mass transport capability [31].

For negative electrodes, hydrogen evolution during charging at high current and/or high SOC results in degradation of the electrodes, possibly via removal of the active oxygen functional groups. A study on pyrolytic graphite showed that the edge planes had more hydrogen evolution activity, while the basal planes degraded more when cycling was carried out to negative potential [32]. This work indicates that further work needs to be conducted to develop negative electrodes with good faradaic efficiency (basal plane) and good stability (edge plane).

3.3. Bipolar Plate Development

Bipolar plates need to have good electronic conductivity, have impermeability to the electrolyte and possess high bending strength (not brittle) while being compatible with the electrolyte. Metal-based bipolar plates undergo corrosion in an acidic environment, while pure graphite bipolar plates are brittle, are relatively porous, allowing leakage between cells, and have high interfacial resistance with felt electrodes [33]. Graphite-based composites with carbon black and other conductive fillers are by far the most predominant choice for vanadium redox flow batteries. Their advantages are high bending strength, low porosity, low interfacial resistance with felt electrodes and low corrosion rates in

an acidic environment. Satola et al. [34] conducted a comprehensive review of bipolar plates that addressed their corrosion, durability and manufacturability. The importance of standardized test procedures to characterize bipolar plate properties such as conductivity and durability was highlighted, and a pathway to increase plate size by more than one order of magnitude using an extrusion process was discussed.

Composite bipolar plates using carbon black in a polymer matrix have demonstrated promising performance at an optimum carbon black content [35] and optimum graphite coating thickness on carbon fabric [35], but these have not gained traction in commercial deployment. It appears that the commercial bipolar plates on the market are sufficiently well developed to meet performance requirements. One of the main developments in bipolar plate design is the incorporation of various flow fields, which is discussed in Section 6.2.

3.4. Electrolyte Development

Simulations at the molecular level using molecular dynamics have enabled the identification of a V^{+5} species existing in a protonated form, which was unstable at 40 °C due to deprotonation. A high acid concentration in a mixture of chloride and sulfate ions was found to mitigate deprotonation by forming contact ion pairs [36]. However, chloride ions interact with the V^{+3} species in the anolyte, leading to precipitation at low temperature. In addition, a special material is needed for compatibility with the mixed-acid electrolyte. The use of bi-additives was effective in mitigating this interaction, allowing for use of the conventional sulfuric acid electrolyte, while increasing the operating temperature range and energy density significantly [37].

Depending on the electrolyte synthesis procedure, which can be performed with either vanadyl sulfate or vanadium pentoxide, different electrolyte volumes will be present at the start of pre-charge, affecting material utilization [38,39]. While high-purity vanadium sources are currently used, the high material cost is detrimental to cost-effective long-duration energy storage applications. The influence of lower-purity electrolytes and specific ions that are detrimental to the performance and life of the battery need to be better understood to further lower the cost of the electrolyte.

4. State of Charge, Crossover and State of Health Estimation

A battery's state of charge estimation is not straightforward since it is affected by coulombic efficiency during charge, energy consumption to support auxiliary load during rest and discharge, and the crossover of vanadium species. Oxygen ingress in the anolyte tank and hydrogen evolution at the negative electrode during charge change the average oxidation state (AOS) of the electrolyte, leading to irreversible capacity loss and a reduction in the state of health. SOC estimation, crossover rates, flow rate optimization and SOH are linked to each other. As an example, accurate SOC estimation allows for the quantification of crossover rates, which, in turn, enables flow rate adjustment to mitigate crossover, with the estimation of AOS enabling SOH estimation. The inter-dependence among SOC, crossover and state of health is covered.

4.1. SOC Estimation

Cell potential measurements do not capture individual half-cell potentials, and hence, are unreliable estimates of SOC, especially considering crossover across the membrane that makes one electrode limiting during charge and the other during discharge. Techniques such as potentiometric titration require withdrawing a sample of electrolyte, and hence, are not practical for an operating system. UV/vis spectroscopy allows for the in-line measurement of SOC but requires expensive equipment and set-up. The measurement of half-cell potentials using reference electrodes allows for the estimation of SOCs in each electrolyte. Electrolyte conductivity, density and viscosity are also proxies for SOC. Half-cell potential measurements coupled with density measurements were used to estimate SOCs

for each half cell [40]. These measurements also accounted for crossover and side reactions to estimate SOH.

Equivalent circuit modeling has been used to estimate SOC, with predicted electrolyte volume changes to estimate capacity fade [41]. Balancing the pressure drop in each half cell by controlling the flow rate in each electrode to be inversely proportional to the average electrolyte viscosity reduced convective electrolyte cross-over and capacity decay [42]. It was also proposed that in addition to flow rate, the permeability of felt electrodes could also be controlled to equalize the pressure drop in each compartment. This work assumed that for such a balanced pressure drop, transfer via diffusion and migration cancel out over a full cycle, ignoring the self-discharge reactions that convert the crossed over V^{+2} and V^{+3} to V^{+4} , and the crossed over V^{+5} and V^{+4} to V^{+3} ; it was also assumed that there would be a reduction in V^{+5} concentration in the positive electrolyte and V^{+2} concentration in the negative electrolyte, and an associated change in the diffusivities of the products.

Vanadium species concentration was estimated in each half cell using an extended Kalman filter (EKF) from the open circuit voltage (OCV) of each half cell measured against a reference cell [43]. This on-line measurement of vanadium species concentration allowed for the control of flow rate to optimize system efficiency, requiring high flow rates at extreme SOC, and lower flow rates near 50% SOC, increasing system efficiency. Flow rate optimization is covered in greater detail in Section 5.1.

4.2. Crossover

As described earlier, a good understanding of crossover pathways and mechanisms is important for accurate SOH estimation.

To address the gap in the data, the transference numbers and diffusion coefficients for all-vanadium species were obtained via measurement of crossover during current flow and open circuit, with V^{+4} , V^{+5} flow on one side at various SOC (including 0% SOC where only V^{+4} was present, and 100% SOC where only V^{+5} was present), and a blank sulfuric acid flow on the other side of a Nafion™ membrane. The experiments were repeated by replacing V^{+4} and V^{+5} with V^{+3} and V^{+2} [44].

The simulation of performance took into account the crossover of species and associated water across the membrane via convection, diffusion and migration [45]. The self-discharge reactions were assumed to occur as soon as the crossover species entered the other compartment. The novelty in this approach was the calculation of the membrane potential as a function of species concentration distribution within the membrane. Under the operating conditions, net species crossover occurred from positive to negative. Using this work, the membrane properties were determined to be critical in determining the net crossover rate of vanadium species using a 2-D model that considered diffusion, migration and convection [46]. Diffusion was reported to be the dominant transport mechanism for Nafion™ membranes, while electro-osmotic convection dominated for sulfonated Radel (s-Radel) membranes (negligible migration and diffusion); this led to a reversal in vanadium crossover between charge and discharge, resulting in lower capacity loss. The higher vanadium crossover rate for s-Radel membrane led to lower coulombic efficiency. Note that convection-related crossover was also significant for Nafion™; however, it always occurred from negative to positive, with the magnitude for discharge an order of magnitude higher than that for charge, while it changed direction for s-Radel. Migration-related crossover for Nafion™ was smaller than for convection, but not negligible. This paper highlights the complexities of species crossover, and the importance of R&D in membrane development. The 2-D model was used to simulate convection-related crossover for four cases where viscosity and flow rates were varied in each compartment. The electro-osmotic contributions to crossover were nearly equal and opposite magnitudes for charge and discharge, while hydraulic convection, incorrectly referred to as osmotic convection by some groups, took place from positive to negative during both charge and discharge; this was related to the higher viscosity of the positive electrolyte. By using asymmetric flow, the pressure drop on either side is made equal, thus eliminating convection-related crossover. Crossover via

diffusion, migration and convection was explored for cation and anion exchange membranes [47], with the advantages of higher conductivity for cation exchange membranes countered by lower crossover rates for anion exchange membranes due to the Donnan exclusion effect.

It was determined that the crossover of vanadium species from negative to positive was greater, resulting in greater consumption of V^{+5} species, and in a lower SOC range on the positive side during cycling [48]. This is because the diffusion coefficient of vanadium species in the membrane is highest for V^{+3} and lowest for VO_2^+ , and is in the following order $V + 3 > VO^{+2}$ or $(V^{+4}) > V + 2 > VO_2^+$ (or V^{+5}) [49]. Rebalancing was carried out by flowing electrolyte through an open circuit to allow mixing via diffusion, and via the active transfer of a portion of the positive electrolyte to the negative; the latter method was more energy efficient, since it could be performed faster, consuming less pumping power.

When migration is not properly accounted for, vanadium crossover occurs from negative to positive due to the higher diffusion coefficient of V^{+2} and V^{+3} . When migration is properly accounted for during discharge, migration occurs from positive to negative, and during charge, it occurs from negative to positive [49]. Hence, during charge, there is a net transfer of vanadium species from positive to negative, and vice versa during discharge. Note that depending on the magnitude of diffusion and migration, for equal charge–discharge duration and current, there would still be net transfer of vanadium species from one electrode to the other. Operation at higher currents increases the contribution due to migration. Hence, depending on the charge–discharge rates, to maintain a balanced electrolyte, the SOC range needs to be restricted. This work provides a tool to operate the flow battery such that the objective of the user is achieved, whether it is high round trip efficiency (RTE), high power or low crossover. The influence of membrane thickness and degradation on crossover was investigated in later work, with the degraded membrane assumed to be 10x the diffusion rate [50], which provides additional insights into BMS for various stack designs and membrane states of health.

Table 1 summarizes transport via diffusion and hydraulic convection, and the total transport for each vanadium species. The table also provides the direction of net vanadium species transfer at the end of each cycle; a positive sign indicates transport from negative to positive, and a negative sign indicates the opposite. While the net transport direction depends on several factors, two out of three cases involve net transfer from negative to positive for Nafion™, and the only reported data for S-PEEK correspond to net transfer from negative to positive. The data corresponding to S-PEEK are identified, and the rest correspond to Nafion™.

Table 1. Direction of vanadium species transport during charge and discharge—data corresponding to S-PEEK are identified, and the rest correspond to Nafion™.

Mode		Charge				Discharge				Net V Transport after Each Cycle
Species		V^{+2}	V^{+3}	V^{+4}	V^{+5}	V^{+2}	V^{+3}	V^{+4}	V^{+5}	
Mechanism	Reference									
Diffusion	[45]		+	-			+	-		
	[46]	+	+	-	-	+	+	-	-	
	[46] S-PEEK	+(negligible)	+(negligible)	-(negligible)	~0	+(negligible)	+(negligible)	-(negligible)	~0	
Hydraulic convection	[49]	+	+	-	-					
	[45]		-	-			+	+(negligible)		
	[46]	+(negligible)	+(negligible)	+(negligible)	+(negligible)	+	+	+	+	
	[46] S-PEEK	-	-	-	-	+		+	+	
Migration	[49]									
	[45]		-	-			+	+		
	[46]	-(negligible)	-(negligible)	-(negligible)	~0	+(negligible)	+(negligible)	+(negligible)	~0	
	[46] S-PEEK	~0	~0	~0	~0	~0		~0	~0	
	[49]	-	-	-	-					

Table 1. Cont.

Mode		Charge				Discharge				Net V Transport after Each Cycle
Species		V ⁺²	V ⁺³	V ⁺⁴	V ⁺⁵	V ⁺²	V ⁺³	V ⁺⁴	V ⁺⁵	
Mechanism	Reference									
Total transport of each species for half cycle	[45]		+	-			+	-		
	[46]	+	+	-	-	+	+	-	+	
	[46] S-PEEK	-	-	-	-	+	+	+	+	
	[49]	+(negligible)	+(negligible)	-	-					
Net V transport after each cycle	[45]									-
	[46]									+
	[46] S-PEEK									+
	[49]									+

Vanadium crossover from negative to positive was found to be dominant for operation at 80 mA/cm², with nearly a 50% capacity loss after 150 cycles, and with the total vanadium concentration increasing from 1.8 M to 2.2 M in the positive electrolyte and decreasing from 1.7 M to 1.2 M in the negative electrolyte. This was accompanied by a decrease in the average oxidation state from 4.8 to 4.4 in the positive electrolyte (<50% SOC) and from 2.2 to 2.1 in the negative electrolyte (>90% SOC) [51]. The rate of capacity loss decreased with each cycle due to the slowing diffusion of vanadium species as the total vanadium concentration gradient across the membrane increased. Using a lower catholyte volume slowed down the capacity decay, with the optimum catholyte volume being 75% of the anolyte volume, and corresponded to the highest average capacity over 160 cycles, thus offering a pathway to increase the energy density and lower crossover-related maintenance using a lower total electrolyte volume.

To quantify the effect of the membrane manufacturing process and pre-treatment, the permeability via diffusion of VO²⁺ was studied for membranes of different thickness produced via dispersion casting or extrusion. Various pre-treatment processes, such as annealing and soaking in water or sulfuric acid, were also examined [52]. The manufacturing process contributed to 3X variation in permeability, while pretreatment contributed to 15X variation. Interestingly, after cycling, the variations in permeability among all membranes disappeared, which indicates that membrane pretreatment and manufacturing processes do not influence the permeability of the membrane towards VO²⁺ and selectivity towards hydrogen ions.

The refractive index of the electrolyte was shown to be a function of total vanadium and sulfate concentration, and SOC [53]. Total vanadium concentration in the catholyte was obtained via titration. During charge, proton transfer to the anolyte leads to a decrease in the catholyte volume. The vanadium concentration obtained via titration at the end of charge was lower than the value computed while taking water transfer into account, which indicates that the vanadium species moved to the anolyte during charge. At the end of discharge, the vanadium species concentration was higher than that occurring due to volume change, which indicates a reverse flow of vanadium to the catholyte from the anolyte.

A 0-D lumped parameter model was developed to simulate vanadium species crossover via diffusion, migration and convection [54]. Crossover via convection was negligible, while migration contributed to 5 to 10%, with diffusion dominating, resulting in the capacity asymptotically approaching a constant value after ~200 cycles. Note that this plateauing of capacity may not happen when migration and convection play a larger role. Some of the parameters, such as membrane electrokinetic permeability and V⁺² diffusivity in the membrane, were obtained via fitting and may need to be experimentally measured. Simulation for various membrane thicknesses showed that power density was higher for thinner membranes, while the limiting current density remained higher for thicker membranes; this was related to the lower crossover and higher reactant concentration in the electrodes.

While the majority of work on electrolyte optimization focuses on increasing specific energy and energy density while maintaining high electrolyte stability across a wide temperature range, Liu et al. [55] showed that lowering the vanadium ion-to-hydrogen ion ratio reduced crossover, thus improving cycling stability. This allowed for operation over a wider temperature range and improved electrolyte utilization, which made it more cost-effective.

Shin, J. et al., used a 3-D model to determine that a net transfer occurred from anolyte to catholyte after a full charge–discharge cycle, taking into account the water that was carried via vanadium species crossover, proton transfer and diffusion, but ignoring migration and convection [56]. Using a lower water concentration and a higher sulfuric acid concentration in the anolyte mitigated net water transfer, while not affecting cell performance, thus mitigating capacity loss. This was validated experimentally in later work [57].

Clearly, research groups have focused on various transport modes—diffusion, migration, hydraulic convection and electro-osmotic transport. Overall, there appears to be a consensus that there is a net transfer of vanadium species from the negative to the positive side. However, the actual transport direction depends on multiple factors, such as membrane type, thickness, SOC range of operation, electrolyte concentration, and current density. A good understanding is needed of the specific system and operating conditions for reliable long-term operation with minimal maintenance.

Table 2 summarizes the modeling work related to crossover, with models ranging from 0-D to 3-D, with and without thermal coupling, with and without water transport being considered, and including one or more of diffusion, migration, hydraulic and electro-osmotic transport of vanadium species across the membrane. Figure 3 shows the various crossover mechanisms during charge and discharge.

Table 2. Summary of models of species crossover in VRFBs.

Reference	[45,46]	[47]	[4]	[50]	[54]	[56]	[58]	[59]	[60]
Model type	2-D	1-D	3-D	3-D	0-D	3-D	1-D	3-D	0-D
Thermal coupling?	No	No	Yes	Yes	No	No	No	No	No
V species transport mechanisms									
Diffusion?	Yes	Yes	Yes	Yes	Yes	Yes	Yes	Yes	Yes
Migration?	Yes	Yes	Yes	Yes	Yes	No	Yes	Yes	Yes
Hydraulic convection of electrolyte due to delta P across membrane?	Yes	No	No	No	Yes	No	No	No	No
Electro-osmotic?	Yes	Yes	No	No	Yes	No	Yes	Yes	Yes
Water transport mechanisms									
Osmotic transport of water?	No	No	No	No	No	No	No	No	No
Transfer of water via electro-osmosis	No	No	No	No	No	Yes	No	No	Yes

4.3. SOH Estimation

One of the factors affecting state of health is the electrode morphology as it ages. As long as the cell potential is kept within its operating window, with a positive electrode potential of less than 1.6 V vs. SCE, O₂ and CO₂ evolution do not take place. However, charging to 1.7 V roughens the electrode surface, which is related to C=O and COOH functional group formation, increasing both the desired reaction rate marginally and the side gas evolution reaction rates significantly, accompanied by lowering of the overpotential [61]. The gas evolution rate, which is the same as the electrode corrosion rate, increases with polarization time and with temperature. While sufficient work has been conducted to optimize the electrode properties for wettability, kinetics and mass transfer, the quantifica-

tion of electrode corrosion rate that contributes to irreversible loss in electrolyte capacity provides an opportunity for research.

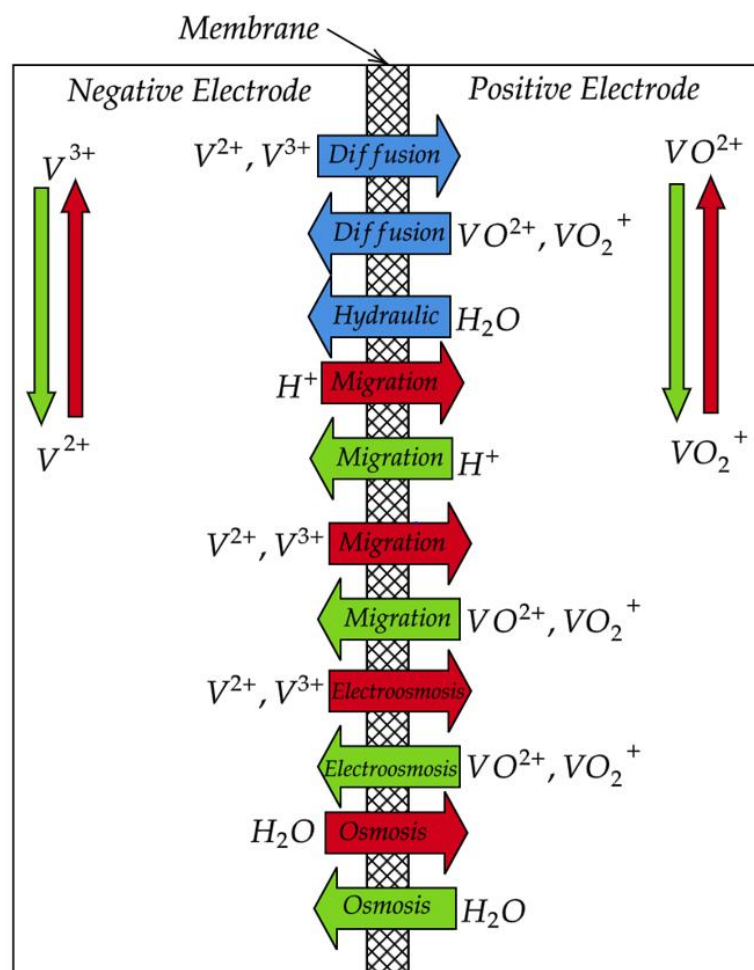


Figure 3. Crossover mechanisms in a vanadium redox flow battery during charge (green arrows) and discharge (red arrows).

For hydraulically parallel electrolyte feed, the overpotential is highest at the port interface with the cell, resulting in high oxidation and reduction currents [62]. This overpotential can be reduced by increasing port resistance, which can mitigate side reactions, such as the generation of CO_2 via the oxidation of felt electrodes, thus reducing felt electrode degradation. This article highlights the fact that reducing shunt current losses also increases the life of felt electrodes.

Measurements of transmitted spectra from the positive electrolyte enable accurate estimation of its SOC in the range of 98–100%, where side reactions are expected to occur [63]. The side reaction intensity as a function of current density was quantified, providing a very useful way to reduce electrolyte loss via side reactions and felt electrode corrosion. The average oxidation state of the electrolyte increases if hydrogen evolution at the negative electrode or oxygen ingress into the anolyte occurs. This increased AOS is accompanied by higher ohmic, charge transfer and mass transfer resistance due to the increase in electrolyte resistivity and viscosity, along with irreversible capacity loss [64].

There has been sufficient work conducted on membrane modifications to reduce crossover while ensuring minimal resistance increase. The modifications range from graphene oxide nanosheets, reducing membrane pore size with silica, and sandwiching a silicate layer between membranes [65–67]. However, none of these studies looked at effect of membrane modification on the degradation of other components. The introduction

of a barrier layer onto a Nafion™ NR212 membrane significantly reduced capacity loss after 250 cycles, with a loss of 50%, compared to 67% for the membrane without a barrier layer [68]. The replacement of the felt electrode allowed the capacity to recover to 91% of its initial value for the membrane with a barrier, while the recovery was only to 54% for the barrier-less membrane. This shows that electrode degradation contributed to 41% of capacity loss for the barrier layer case, while it contributed to only 21% of capacity loss for the barrier-less membrane. This study shows the importance of understanding the mechanism that contributes to the degradation of stack components such as felt electrodes while trying to solve the crossover issue.

A very effective experimental technique was developed to calculate the average oxidation state of an electrolyte using an OCV cell and determining the number of plateaus [69]. A two-plateau system had an AOS of 3.5, while a three-plateau system had an AOS less than or greater than 3.5. Based on the plateau voltage, it could be determined that the AOS was $<$ or $>$ 3.5. However, the plateau voltage drift could lead to errors in the AOS estimation. This was circumvented by looking at the derivative of OCV with respect to time ($dOCV/dt$), with a steeper value corresponding to V^{+3} to V^{+4} on the positive side, and a less steep value of V^{+4} to V^{+3} on the negative side. If the less steep peak occurred first, $AOS < 3.5$, and vice versa. This was tested using solutions of different AOS in a laboratory single cell and in a stack, with an estimation error of $<4\%$.

Di Noto et al. [70] considered the complexity of the all-vanadium chemistry, accounting for the multiple vanadium species and associated adverse reactions, to fully understand and reduce its capacity loss by proposing approaches to reduce undesired reactions, which can further help in ensuring optimal operation.

5. Battery Management System

5.1. Flow Optimization

Different strategies have been used to optimize flow in a redox flow battery. Using a fixed stoichiometric flow rate, the flow rate increases during charge or discharge as the reactant concentration decreases. Some approaches are based on physics-based models that ignore mass transport and shunt current losses [71], while these losses are considered in other models [5,72,73]. The estimation of the limiting current during operation allowed for the optimization of flow rate to ensure the maximization of input energy from a renewable wind source after accounting for pumping losses; the average current in each time step was used as an input to calculate the optimum flow rate in the next time step [74], while ensuring the SOC and flow rate did not cross the minimum and maximum limits. In this work, the results for minimum flow rate were better than those for maximum flow rate due to lower pumping losses, but this is simply due to the values of minimum and maximum flow rates chosen. This highlights the importance of the chosen operating envelope.

5.2. Operation Strategy

The implementation of an approach to maximize self-consumption for a residential 3.24 kW photovoltaic (PV) array paired with a 5 kW and 60 kWh vanadium redox flow battery was performed—with no power injected to the grid and 25% of the energy supplied by PV, within a range of 0–100% SOC—while accounting for varying charge and discharge power as a function of SOC [75]. To improve RTE, it was determined that the DC operating voltage range of the battery needs to be compatible with the efficient operating range of the inverter. In a later work, the group included ramp control along with self-consumption maximization as a second energy management approach, with a third approach taking into account the 24 h forward-looking weather forecast to optimize night-time charging [76]. The simulation was successful in maintaining a PV ramp rate below 10% of the rated power per minute, with a self-consumption rate close to 60%, while improving grid reliability.

Parmeshwarappa, P. et al. determined that the average charge power is three times that of the average discharge power when a flow battery is coupled with rooftop solar panels, with a peak power ratio equal to 4.7 [77]. Hence, the battery charging is more

severe, with the stack sizing and flow rate optimized for charging. With the SOC range set to 20–90%, the flow rate needs to be increased significantly at the higher end of the SOC range to support the charge power.

A model to minimize voltage loss and crossover-related capacity loss was developed by applying different weighting factors to the type of loss [78]. As expected, a higher flow rate minimized voltage loss, and a lower flow rate minimized crossover-related capacity loss. The novelty of this approach is that depending on the chosen objective functions (capital cost minimization versus levelized cost minimization versus energy throughput maximization), different weighting factors can be assigned to capacity loss and voltage loss/overpotential. In general, flow rate control has to be tailored to the end user's preferred objective function.

6. Stack Design

6.1. Stack Sizing and Architecture

One of the earlier papers on system design included specifications, design details, and an estimation of cost, with stack sizing performed based on the required total current and current density; the electrolyte volume estimation was performed using the number of moles required and the associated concentration [79].

A MATLAB model was developed to size a redox flow battery connected to a 13 kW PV array. The vanadium charged species concentration in the stack and tanks was used to estimate the current based on the difference between solar array generation and load [80]. Model validation with experimental data was followed by optimization of the stack and tank size to support the load at the target efficiency. A detailed analysis of capital cost and performance characterization of redox flow batteries were used to optimally size redox flow batteries for residences with PV arrays, taking into account market prices [81].

A tubular design, with advantages related to scalable manufacturing, was found to have much lower sealing length, but had a current density an order of magnitude lower due to high ohmic resistance, while the activation and mass transfer resistance were comparable to a planar design [82].

6.2. Flow Field Design

A performance comparison of serpentine and interdigitated flow fields was performed experimentally and using finite element analysis [83]. At low flow rates, the interdigitated flow field showed better performance in the 250–500 mA/cm² range, with a more uniform flow and current distribution, which was further verified by thermal imaging. As flow rate was increased, the gap in performance decreased at the same current density, but the serpentine flow field had a much greater pressure drop. For a fixed flow rate, increasing the electrode thickness led to an improvement in performance for both designs, followed by a performance reduction with a further increase in thickness. The gap in performance decreased with increasing electrode thickness, mainly due to lower velocity through the porous electrode at larger electrode thicknesses. This study showed the importance of flow field design, felt electrode thickness and flow rate in determining which design is preferred at various current and power densities. Felt electrode treatment to improve kinetics is an additional parameter that allows the use of thinner felt, and hence, results in a higher velocity through the electrode for the interdigitated design. Another study showed that serpentine flow design had the lowest pressure drop, followed by the interdigitated design and the flow-through design [84]. It should be noted that there was no header at the inlet or outlet, which favored the serpentine design and eliminated the advantage of the interdigitated design. While the conventional flow-through design would still be expected to have the highest pressure drop, the presence of the headers would direct the flow more uniformly, thus improving performance and reducing pressure drop at a fixed flow rate. Three-dimensional finite element modeling showed that performance and pressure drop for serpentine electrodes was higher at a fixed flow rate compared to the interdigitated flow field [85]. Accounting for higher pumping losses, the interdigitated flow field design

provided greater system efficiency. The reactant, current and SOC distribution were found to be more uniform for the interdigitated design, with these factors affected by electrode permeability and specific surface area. A comprehensive review of the effectiveness of various flow fields was performed [86,87]. A detailed analysis of interdigitated flow field channel dimensions and rib width that minimized system costs was performed for a fixed SOC operating range for a system with various durations [88], with a focus on the positive half-cell whose kinetics are faster, and hence, mass transport becomes dominant.

Flow pattern analysis for serpentine flow fields of varying channel widths and heights and rib widths was conducted. For smaller channel and rib widths, cross-flow through porous electrodes was dominant, while flow through channels dominated for larger channel and rib widths [89]. Simulations underestimated the pressure drop, which was attributed to uncompressed felt electrodes in the channels. When accounting for this and adjusting for lower permeability of the compressed region under the ribs, the experimental results were in good agreement with the simulations.

6.3. Electrode Design for Various Flow Fields

The significance of ohmic, activation and mass transport polarization was investigated via modeling for serpentine and interdigitated flow designs [90]. The performance increased with specific area up to a certain limit, after which mass transfer dominated; a further performance increase required a larger fiber diameter and higher porosity to improve mass transport. The optimum specific surface area, fiber diameter and porosity depended on the flow field design and the applied current density. For example, at a lower current density, mass transfer limitations were not significant, favoring a high specific surface area. At a higher current density, graded porosity along the electrode thickness and along the flow path distributed the current uniformly throughout the electrode. Increasing the fiber diameter significantly increased electrolyte velocity in the electrode in the serpentine case, reducing mass transfer overpotential, while the pressure drop was reduced for interdigitated flow.

Gundlapalli, R. et. al., determined that increasing electrode size led to higher system efficiency due to lower pumping losses because the number of channels feeding the stack was reduced for a fixed power level [91]. So, in addition to dimensions for flow channel width and depth and rib width, electrode sizing positively impacts performance and manufacturing scalability.

The effects of electrode shape and flow field were investigated [92], which resulted in findings that circular electrodes have the most uniform flow distribution and the lowest pressure drop, followed by rhomboidal and square. The parallel flow field design has the lowest pressure drop for circular electrodes, followed by the flow-through and serpentine designs.

Laboratory experiments commonly use high flow rates to maximize DC performance; however, the flow rate per ampere for larger electrodes in commercial stacks is typically maintained at lower levels to reduce pumping losses. The porosity gradient in the catalyst layer has been explored in the fuel cell space to ensure a sufficient reactant gas delivery rate to the active sites. However, this has not been explored for flow batteries within felt electrodes. A proxy for higher porosity is larger fiber diameter, with the associated reduction in specific surface area countered by appropriate surface treatment [90].

The effect of the compression of electrodes on performance was also investigated [93]. Performance improvement related to improved contact resistance was observed at 20% compression, while mass transport and pumping losses dominated at >25% compression, thus demonstrating a 20–25% compression ratio as optimum.

7. Environmental Impact

While performance and life have been the main criteria for material and process selection to manufacture flow batteries, the importance of considering environmental impact was highlighted [94]. Eight categories were used to characterize different flow

battery chemistries, namely, global warming potential, the depletion of abiotic or natural resources, ozone depletion potential, freshwater ecotoxicity, fine particulate matter, acidification potential, algae growth in freshwater (also known as eutrophication) and cumulative fossil fuel energy demand. Iron flow batteries had the lowest environmental impact in the six categories, while vanadium redox flow batteries had the highest impact in the six categories. Zinc bromine batteries had the highest impact on the depletion of abiotic or natural resources, and the lowest impact on ozone depletion and freshwater ecotoxicity. Using alternate materials and processes, each technology showed potential for reducing environmental impact. For example, the global warming potential of vanadium redox flow batteries can be reduced by 67% using an alternative process for vanadium pentoxide extraction and by replacing Nafion™ to reduce ozone depletion, while replacing polymer resins with alternate materials could lower the ecotoxicity of iron flow batteries.

8. Conclusions

A review of the gaps in all-vanadium redox flow battery development was conducted and pathways were provided to address them and facilitate deployment for durations extending to >24 h. The importance of reduced-order physics-based models or analytical models for implementation in a BMS was highlighted. The use of the Monte Carlo method to generate various porous electrode geometries and enable the simulation of a diverse range of porous electrodes, and of the lattice Boltzmann method to validate hydraulic models, was identified to be important in reducing simulation time and validating existing models.

In the area of material development, S-PEEK with an optimized sulfation degree was identified to be the most viable alternative to Nafion™ membranes, while anion exchange membranes, despite their lower conductivity, were identified as a good choice for LDES if their durability in an acidic environment can be increased.

Material properties for bipolar plates were not addressed in detail, since commercial bipolar plates comprising graphite composites with carbon black and other conductive fillers meet performance and durability requirements. The main area for additional development was matching flow fields with porous felt properties, such as permeability, such that at the maximum flow rate available for the system, and the velocity of the electrolyte at high SOC during charge and low SOC during discharge, is sufficiently high to overcome mass transfer limitations in the design of the SOC operating range.

The impact of molecular-level modeling for electrolyte development was highlighted by providing examples of mixed-acid electrolytes to minimize the de-protonation of V^{+5} species, and the use of bi-additives to expand the temperature range of operation at higher electrolyte concentrations.

The inter-dependance of SOC, crossover and SOH was described, offering insights on the mitigation of reversible and irreversible capacity loss via power and flow control; this is to ensure voltages stay below gassing levels and crossover is minimized while obtaining good performance, especially at extreme SOCs, by ensuring sufficient velocity through the felt electrode and facilitate mass transport. In other words, opposing factors, such as enhanced mass transport and crossover mitigation, need to be balanced against each other.

For electrodes, matching the permeability with the bipolar flow field to ensure sufficient velocity and ensure good mass transfer was identified as crucial to improving electrolyte utilization across the 6–24+ hour duration where flow batteries are best deployed. To address hydrogen evolution at the negative electrode towards the end of charge, which causes irreversible capacity loss, areas for developmental work to improve high faradaic efficiency (basal plane) and durability (edge plane) were identified.

Tailoring electrode properties to various current densities was also discussed. As an example, increasing the fiber diameter reduces the pressure drop at a fixed flow rate, while also reducing the surface area. Having a high surface area at the expense of high pressure drop at a fixed flow rate leads to mass transport losses at a high current density, and a low surface area leads to high activation losses. Hence, the surface treatment of electrodes with

optimum fiber diameters to enhance surface area and permeability, while maintaining high velocity at extreme SOCs during charge or discharge, is important.

The environmental impact of each technology needs to be considered, along with its performance and durability, to gain a holistic understanding of the technology's true positive and negative impacts on storing and dispatching clean electricity.

Author Contributions: Conceptualization: V.V.V., A.J.C., E.C.T. and D.M.R.; writing—original draft preparation: V.V.V., A.J.C. and D.M.R.; writing—review and editing: V.V.V., Q.H., N.S. and G.L.; supervision: D.M.R.; funding acquisition, D.M.R. All authors have read and agreed to the published version of the manuscript.

Funding: This work was funded by the U.S. Department of Energy (DOE), Office of Electricity (OE), under contract DE-AC06-76LO1830 through the Pacific Northwest National Laboratory (Validated Safety & Reliability, project #70249). The Pacific Northwest National Laboratory is operated by Battelle for the DOE under Contract DE-AC05-76RL01830.

Institutional Review Board Statement: Not applicable.

Informed Consent Statement: Informed consent was obtained from all subjects involved in the study.

Data Availability Statement: Not applicable as this is an overview.

Acknowledgments: The authors would like to acknowledge Vincent Sprenkle for his overall guidance, and Mark E. Gross for supporting the establishment of the reliability testing lab at PNNL.

Conflicts of Interest: The authors declare no conflict of interest.

References

1. U.S. Department of Energy Office of Clean Energy Demonstrations. Biden-Harris Administration Announces Nearly \$350 Million for Long-Duration Energy Storage Demonstration Projects. 2022. Available online: <https://www.energy.gov/articles/biden-harris-administration-announces-nearly-350-million-long-duration-energy-storage> (accessed on 29 January 2023).
2. Sun, C.; Chen, J.; Zhang, H.; Han, C.; Luo, Q. Hybrid inorganic-organic proton-conducting membranes based on SPEEK doped with WO₃ nanoparticles for application in vanadium redox flow batteries. *Electrochim. Acta* **2019**, *309*, 311–325. [CrossRef]
3. Sangwon, K. Vanadium Redox Flow Batteries: Electrochemical Engineering. In *Energy Storage Devices*; Demirkan, M., Adel, A., Eds.; IntechOpen: Rijeka, Croatia, 2019; Chapter 7.
4. Huang, Z.; Mu, A.; Wu, L.; Yang, B.; Qian, Y.; Wang, J. Comprehensive Analysis of Critical Issues in All-Vanadium Redox Flow Battery. *ACS Sustain. Chem. Eng.* **2022**, *10*, 7786–7810. [CrossRef]
5. Reed, D.; Thomsen, E.; Li, B.; Wang, W.; Nie, Z.; Koeppl, B.; Kizewski, J.; Sprenkle, V. Stack Developments in a kW Class All Vanadium Mixed Acid Redox Flow Battery at the Pacific Northwest National Laboratory. *J. Electrochem. Soc.* **2016**, *163*, A5211. [CrossRef]
6. Viswanathan, V.; Crawford, A.; Stephenson, D.; Kim, S.; Wei, W.; Bin, L.; Coffey, G.; Thomsen, E.; Gordon, G.; Balducci, P.; et al. Cost and performance model for redox flow batteries. *J. Power Sources* **2014**, *247*, 1040–1051. [CrossRef]
7. Crawford, A.; Viswanathan, V.; Stephenson, D.; Wang, W.; Thomsen, E.; Reed, D.; Li, B.; Balducci, P.; Kintner-Meyer, M.; Sprenkle, V. Comparative analysis for various redox flow batteries chemistries using a cost performance model. *J. Power Sources* **2015**, *293*, 388–399. [CrossRef]
8. Ma, R.X.; Seltzer, B.P.; Gong, K.; Shuang, G.; Yushan, Y. A General, Analytical Model for Flow Battery Costing and Design. *J. Electrochem. Soc.* **2018**, *165*, A2209. [CrossRef]
9. Viswanathan, V.; Mongird, K.; Franks, R.; Li, X.; Sprenkle, V. *Grid Energy Storage Technology Cost and Performance Assessment*; Pacific Northwest National Laboratory: Richland, WA, USA, 2022.
10. Zhang, H.; Sun, C.; Ge, M. Review of the Research Status of Cost-Effective Zinc–Iron Redox Flow Batteries. *Batteries* **2022**, *8*, 202. [CrossRef]
11. Iwakiri, I.; Antunes, T.; Almeida, H.; Sousa, J.P.; Figueira, R.B.; Mendes, A. Redox Flow Batteries: Materials, Design and Prospects. *Energies* **2021**, *14*, 5643. [CrossRef]
12. Petek, T.J.; Hoyt, N.C.; Savinell, R.F.; Wainright, J.S. Slurry electrodes for iron plating in an all-iron flow battery. *J. Power Sources* **2015**, *294*, 620–626. [CrossRef]
13. Duduta, M.; Ho, B.; Wood, V.C.; Limthongkul, P.; Brunini, V.E.; Carter, W.C.; Chiang, Y.-M. Semi-Solid Lithium Rechargeable Flow Battery. *Adv. Energy Mater.* **2011**, *1*, 511–516. [CrossRef]
14. Qi, Z.; Liu, A.; Koenig, G. Carbon-free Solid Dispersion LiCoO₂ Redox Couple Characterization and Electrochemical Evaluation for All Solid Dispersion Redox Flow Batteries. *Electrochim. Acta* **2017**, *228*, 91–99. [CrossRef]

15. Cheng, Y.; Wang, X.; Huang, S.; Samarakoon, W.; Xi, S.; Ji, Y.; Zhang, F.; Du, Y.; Feng, Z.; Adams, S.; et al. Redox Targeting-Based Vanadium Redox-Flow Battery. *ACS Energy Lett.* **2019**, *4*, 3028–3035. [CrossRef]
16. Yan, R.; Wang, Q. Redox-Targeting-Based Flow Batteries for Large-Scale Energy Storage. *Adv. Mater.* **2018**, *30*, e1802406. [CrossRef] [PubMed]
17. Li, Y.; Van Nguyen, T.A. Solid/Liquid High-Energy-Density Storage Concept for Redox Flow Batteries and Its Demonstration in an H₂-V System. *J. Electrochem. Soc.* **2022**, *169*, 110509. [CrossRef]
18. Puleston, T.; Clemente, A.; Costa-Castelló, R.; Serra, M. Modelling and Estimation of Vanadium Redox Flow Batteries: A Review. *Batteries* **2022**, *8*, 121. [CrossRef]
19. Clemente, A.; Costa-Castelló, R. Redox Flow Batteries: A Literature Review Oriented to Automatic Control. *Energies* **2020**, *13*, 4514. [CrossRef]
20. Vynnycky, M. Analysis of a model for the operation of a vanadium redox battery. *Energy* **2011**, *36*, 2242–2256. [CrossRef]
21. Chen, Y.; Xu, Z.; Wang, C.; Bao, J.; Koeppe, B.; Yan, L.; Gao, P.; Wang, W. Analytical modeling for redox flow battery design. *J. Power Sources* **2021**, *482*, 228817. [CrossRef]
22. Li, Y.; Skyllas-Kazacos, M.; Bao, J. A dynamic plug flow reactor model for a vanadium redox flow battery cell. *J. Power Sources* **2016**, *311*, 57–67. [CrossRef]
23. Xu, Q.; Zhao, T. Fundamental models for flow batteries. *Prog. Energy Combust. Sci.* **2015**, *49*, 40–58. [CrossRef]
24. Poly Processing Solutions Simplified. Vertical Tanks. Available online: <https://www.polyprocessing.com/tank-specifications/our-tank-offerings/vertical-tanks/> (accessed on 13 January 2023).
25. Shi, Y.; Eze, C.; Xiong, B.; He, W.; Zhang, H.; Lim, T.M.; Ukil, A.; Zhao, J. Recent development of membrane for vanadium redox flow battery applications: A review. *Appl. Energy* **2019**, *238*, 202–224. [CrossRef]
26. Thiam, B.G.; Vaudreuil, S. Review—Recent Membranes for Vanadium Redox Flow Batteries. *J. Electrochem. Soc.* **2021**, *168*, 070553. [CrossRef]
27. Thiam, B.G.; El Magri, A.; Vaudreuil, S. An overview on the progress and development of modified sulfonated polyether ether ketone membranes for vanadium redox flow battery applications. *High Perform. Polym.* **2021**, *34*, 131–148. [CrossRef]
28. Mazur, P.; Mrlik, J.; Pocedic, J.; Vrana, J.; Dundalek, J.; Kosek, J.; Bystron, T. Effect of graphite felt properties on the long-term durability of negative electrode in vanadium redox flow battery. *J. Power Sources* **2019**, *414*, 354–365. [CrossRef]
29. He, Z.; Lv, Y.; Zhang, T.; Zhu, Y.; Dai, L.; Yao, S.; Zhu, W.; Wang, L. Electrode materials for vanadium redox flow batteries: Intrinsic treatment and introducing catalyst. *Chem. Eng. J.* **2022**, *427*, 131680. [CrossRef]
30. Gencten, M.; Sahin, Y. A critical review on progress of the electrode materials of vanadium redox flow battery. *Int. J. Energy Res.* **2020**, *44*, 7903–7923. [CrossRef]
31. Maleki, M.; El-Nagar, G.A.; Bernsmeier, D.; Schneider, J.; Roth, C. Fabrication of an efficient vanadium redox flow battery electrode using a free-standing carbon-loaded electropunk nanofibrous composite. *Sci. Rep.* **2020**, *10*, 11153. [CrossRef] [PubMed]
32. Taylor, S.M.; Pătru, A.; Perego, D.; Fabbri, E.; Schmidt, T.J. Influence of Carbon Material Properties on Activity and Stability of the Negative Electrode in Vanadium Redox Flow Batteries: A Model Electrode Study. *ACS Appl. Energy Mater.* **2018**, *1*, 1166–1174. [CrossRef]
33. Gautam, R.K.; Kumar, A. A review of bipolar plate materials and flow field designs in the all-vanadium redox flow battery. *J. Energy Storage* **2022**, *48*, 104003. [CrossRef]
34. Satola, B. Review—Bipolar Plates for the Vanadium Redox Flow Battery. *J. Electrochem. Soc.* **2021**, *168*, 060503. [CrossRef]
35. Kim, K.H.; Kim, B.; Lee, D. Development of carbon composite bipolar plate (BP) for vanadium redox flow battery (VRFB). *Compos. Struct.* **2014**, *109*, 253–259. [CrossRef]
36. Murugesan, V.; Li, L.; Gordon, G.; Liu, J.; Zhang, H.; Yang, Z.; Hu, J.Z. Towards understanding the poor thermal stability of V⁵⁺ electrolyte solution in Vanadium Redox Flow Batteries. *J. Power Sources* **2011**, *196*, 3669–3672.
37. Murugesan, V.; Zimin, N.; Zhang, X.; Gao, P.; Zhu, Z.; Huang, Q.; Yan, L.; Reed, D.; Wang, W. Accelerated design of vanadium redox flow battery electrolytes through tunable solvation chemistry. *Cell Rep. Phys. Sci.* **2021**, *2*, 100323. [CrossRef]
38. Choi, C.; Kim, S.; Kim, R.; Choi, Y.; Kim, S.; Jung, H.-Y.; Yang, J.H.; Kim, H.-T. A review of vanadium electrolytes for vanadium redox flow batteries. *Renew. Sustain. Energy Rev.* **2017**, *69*, 263–274. [CrossRef]
39. Roznyatovskaya, N.; Noack, J.; Mild, H.; Fühl, M.; Fischer, P.; Pinkwart, K.; Tübke, J.; Skyllas-Kazacos, M. Vanadium Electrolyte for All-Vanadium Redox-Flow Batteries: The Effect of the Counter Ion. *Batteries* **2019**, *5*, 13. [CrossRef]
40. Truckmen, T.; Kuhn, P.; Ressel, S. A combined in situ monitoring approach for half-cell state of charge and state of health of vanadium redox flow batteries. *Electrochim. Acta* **2020**, *362*, 137174.
41. Khaki, B.; Das, P. Fast and Simplified Algorithms for SoC and SoH Estimation of Vanadium Redox Flow Batteries. In Proceedings of the 2021 IEEE Green Technologies Conference (GreenTech), Denver, CO, USA, 7–9 April 2021.
42. Song, Y.; Li, X.; Xiong, J.; Yang, L.; Pan, G.; Yan, C.; Tang, A. Electrolyte transfer mechanism and optimization strategy for vanadium flow batteries adopting a Nafion membrane. *J. Power Sources* **2020**, *449*, 227503. [CrossRef]
43. Jienkulsawad, P.; Jirabovornwisut, T.; Chen, Y.-S.; Arpornwichanop, A. Improving the Performance of an All-Vanadium Redox Flow Battery under Imbalance Conditions: Online Dynamic Optimization Approach. *ACS Sustain. Chem. Eng.* **2020**, *8*, 13610–13622. [CrossRef]
44. Vardner, J.T.; Ye, A.A.; Valdes, D.A.; West, A.C. Current-Driven Vanadium Crossover as a Function of SOC and SOD in the Vanadium Redox Flow Battery. *J. Electrochem. Soc.* **2020**, *167*, 080512. [CrossRef]

45. Knehr, K.W.; Agar, E.; Dennison, C.R.; Kalidindi, A.R.; Kumbur, E.C. A Transient Vanadium Flow Battery Model Incorporating Vanadium Crossover and Water Transport through the Membrane. *J. Electrochem. Soc.* **2012**, *159*, A1446. [[CrossRef](#)]
46. Agar, E.; Knehr, K.W.; Chen, D.; Hickner, M.A.; Kumbur, E.C. Species transport mechanisms governing capacity loss in vanadium flow batteries: Comparing Nafion and sulfonated Radel membranes. *Electrochim. Acta* **2013**, *98*, 66–74. [[CrossRef](#)]
47. Haisch, T.; Ji, H.; Holtz, L.; Struckmann, T.; Weidlich, C. Half-Cell State of Charge Monitoring for Determination of Crossover in VRFB—Considerations and Results Concerning Crossover Direction and Amount. *Membranes* **2021**, *11*, 232. [[CrossRef](#)] [[PubMed](#)]
48. Luo, Q.; Li, L.; Wang, W.; Nie, Z.; Wei, X.; Li, B.; Chen, B.; Yang, Z.; Sprenkle, V. Capacity Decay and Remediation of Nafion-based All-Vanadium Redox Flow Batteries. *ChemSusChem* **2013**, *6*, 268–274. [[CrossRef](#)]
49. Oh, K.; Won, S.; Ju, H. A comparative study of species migration and diffusion mechanisms in all-vanadium redox flow batteries. *Electrochim. Acta* **2015**, *181*, 238–247. [[CrossRef](#)]
50. Won, S.; Oh, K.; Ju, H. Numerical analysis of vanadium crossover effects in all-vanadium redox flow batteries. *Electrochim. Acta* **2015**, *177*, 310–320. [[CrossRef](#)]
51. Park, J.H.; Park, J.J.; Park, O.O.; Yang, J.H. Capacity Decay Mitigation by Asymmetric Positive/Negative Electrolyte Volumes in Vanadium Redox Flow Batteries. *ChemSusChem* **2016**, *9*, 3181–3187. [[CrossRef](#)] [[PubMed](#)]
52. Xie, W.; Darling, R.; Perry, M. Processing and Pretreatment Effects on Vanadium Transport in Nafion Membranes. *J. Electrochem. Soc.* **2016**, *163*, A5084. [[CrossRef](#)]
53. Zhang, Y.; Ma, K.; Kuang, X.; Liu, L.; Sun, Y.; Xi, J. Real-Time Study of the Disequilibrium Transfer in Vanadium Flow Batteries at Different States of Charge via Refractive Index Detection. *J. Phys. Chem. C* **2018**, *122*, 28550–28555. [[CrossRef](#)]
54. Boettcher, P.A.; Agar, E.; Dennison, C.R.; Kumbur, E.C. Modeling of Ion Crossover in Vanadium Redox Flow Batteries: A Computationally-Efficient Lumped Parameter Approach for Extended Cycling. *J. Electrochem. Soc.* **2016**, *163*, A5244. [[CrossRef](#)]
55. Liu, Y.; Yu, L.; Loi, L.; Xi, J. Tailoring the vanadium/proton ratio of electrolytes to boost efficiency and stability of vanadium flow batteries over a wide temperature range. *Appl. Energy* **2021**, *301*, 117454. [[CrossRef](#)]
56. Shin, J.; Jeong, B.; Chinannai, M.F.; Ju, H. Mitigation of water and electrolyte imbalance in all-vanadium redox flow batteries. *Electrochim. Acta* **2021**, *390*, 138858. [[CrossRef](#)]
57. Shin, J.; Kim, C.; Jeong, B.; Vaz, N.; Ju, H. New operating strategy for all-vanadium redox flow batteries to mitigate electrolyte imbalance. *J. Power Sources* **2022**, *526*, 231144. [[CrossRef](#)]
58. Darling, R.M.; Weber, A.Z.; Tucker, M.C.; Perry, M.L. The Influence of Electric Field on Crossover in Redox-Flow Batteries. *J. Electrochem. Soc.* **2016**, *163*, A5014. [[CrossRef](#)]
59. Hao, L.; Wang, Y.; He, Y. Modeling of Ion Crossover in an All-Vanadium Redox Flow Battery with the Interfacial Effect at Membrane/Electrode Interfaces. *J. Electrochem. Soc.* **2019**, *166*, A1310. [[CrossRef](#)]
60. Schafner, K.; Becker, M.; Turek, T. Capacity balancing for vanadium redox flow batteries through continuous and dynamic electrolyte overflow. *J. Appl. Electrochem.* **2021**, *51*, 1217–1228. [[CrossRef](#)]
61. Liu, H.; Xu, W.; Yan, C.; Qiao, Y. Corrosion behavior of a positive graphite electrode in vanadium redox flow battery. *Electrochim. Acta* **2011**, *56*, 8783–8790. [[CrossRef](#)]
62. Darling, R.M.; Shiao, H.-S.; Weber, A.Z.; Perry, M.L. The Relationship between Shunt Currents and Edge Corrosion in Flow Batteries. *J. Electrochem. Soc.* **2017**, *164*, E3081. [[CrossRef](#)]
63. Liu, L.; Li, Z.; Xi, J.; Zhou, H.; Wu, Z.; Qiu, X. Rapid detection of the positive side reactions in vanadium flow batteries. *Appl. Energy* **2017**, *185*, 452–462. [[CrossRef](#)]
64. Nourani, M.; Dennison, C.R.; Jin, X.; Liu, F.; Agar, E. Elucidating Effects of Faradaic Imbalance on Vanadium Redox Flow Battery Performance: Experimental Characterization. *J. Electrochem. Soc.* **2019**, *166*, A3844. [[CrossRef](#)]
65. Yu, L.; Lin, F.; Xu, L.; Xi, J. A recast Nafion/graphene oxide composite membrane for advanced vanadium redox flow batteries. *RSC Adv.* **2016**, *6*, 3756–3763. [[CrossRef](#)]
66. Zhang, H.; Zhang, H.; Li, X.; Mai, Z.; Wei, W. Silica modified nanofiltration membranes with improved selectivity for redox flow battery application. *Energy Environ. Sci.* **2012**, *5*, 6299–6303. [[CrossRef](#)]
67. Kim, J.; Jeon, J.-D.; Kwak, S.-Y. Nafion-based composite membrane with a permselective layered silicate layer for vanadium redox flow battery. *Electrochem. Commun.* **2014**, *38*, 68–70. [[CrossRef](#)]
68. Cecchetti, M.; Ebaugh, T.A.; Yu, H.; Bonville, L.; Gambaro, C.; Meda, L.; Maric, R.; Casalegno, A.; Zago, M. Design and Development of an Innovative Barrier Layer to Mitigate Crossover in Vanadium Redox Flow Batteries. *J. Electrochem. Soc.* **2020**, *167*, 130535. [[CrossRef](#)]
69. Beyer, K.; Gross Austing, J.; Satola, B.; Di Nardo, T.; Zobel, M.; Agert, C. Electrolyte Imbalance Determination of a Vanadium Redox Flow Battery by Potential-Step Analysis of the Initial Charging. *ChemSusChem* **2020**, *13*, 2066–2071. [[CrossRef](#)] [[PubMed](#)]
70. Di Noto, V.; Vezzu, K.; Crivellaro, G.; Pagot, G.; Sun, C.; Meda, L.; Rutkowska, I.A.; Kulesza, P.J.; Zawodzinski, T.A. A general electrochemical formalism for vanadium redox flow batteries. *Electrochim. Acta* **2022**, *408*, 139937. [[CrossRef](#)]
71. Blanc, C.; Rufer, A. Optimization of the operating point of a vanadium redox flow battery. In Proceedings of the 2009 IEEE Energy Conversion Congress and Exposition, San Jose, CA, USA, 20–24 September 2009.
72. Tang, A.; Bao, J.; Skyllas-Kazacos, M. Studies on pressure losses and flow rate optimization in vanadium redox flow battery. *J. Power Sources* **2014**, *248*, 154–162. [[CrossRef](#)]
73. König, S.; Suriyah, M.; Leibfried, T. Innovative model-based flow rate optimization for vanadium redox flow batteries. *J. Power Sources* **2016**, *333*, 134–144. [[CrossRef](#)]

74. Akter, M.P.; Li, Y.; Bao, J.; Skyllas-Kazacos, M.; Rahman, M.F. Optimal Charging of Vanadium Redox Flow Battery with Time-Varying Input Power. *Batteries* **2019**, *5*, 20. [[CrossRef](#)]
75. Fialho, L.; Fartaria, T.; Narvarate, L.; Collares Pereira, M. Implementation and Validation of a Self-Consumption Maximization Energy Management Strategy in a Vanadium Redox Flow BIPV Demonstrator. *Energies* **2016**, *9*, 496. [[CrossRef](#)]
76. Foles, A.; Fialho, L.; Collares Pereira, M.; Horta, P. An approach to implement photovoltaic self-consumption and ramp-rate control algorithm with a vanadium redox flow battery day-to-day forecast charging. *Sustain. Energy Grids Netw.* **2022**, *30*, 100626. [[CrossRef](#)]
77. Parmeshwarappa, P.; Gundlapalli, R.; Jayanti, S. Power and Energy Rating Considerations in Integration of Flow Battery with Solar PV and Residential Load. *Batteries* **2021**, *7*, 62. [[CrossRef](#)]
78. Khaki, B.; Das, P. Voltage loss and capacity fade reduction in vanadium redox battery by electrolyte flow control. *Electrochim. Acta* **2022**, *405*, 139842. [[CrossRef](#)]
79. Moore, M.; Watson, J.; Zawodzinski, T.A.; Counce, R.; Kamath, H. A Step by Step Design Methodology for an All-Vanadium Redox-Flow Battery. *Chem. Eng. Educ.* **2012**, *46*, 239.
80. Gibson, C.; Morrissey, K.G. A New Design Method for Vanadium Redox Batteries in Renewable Energy Systems. *Inq. Univ. Ark. Undergrad. Res. J.* **2015**, *18*, 6.
81. Zhang, X.; Li, Y.; Skyllas-Kazacos, M.; Bao, J. Optimal Sizing of Vanadium Redox Flow Battery Systems for Residential Applications Based on Battery Electrochemical Characteristics. *Energies* **2016**, *9*, 857. [[CrossRef](#)]
82. Ressel, S.; Laube, A.; Fischer, S.; Chica, A.; Flower, T.; Struckmann, T. Performance of a vanadium redox flow battery with tubular cell design. *J. Power Sources* **2017**, *355*, 199–205. [[CrossRef](#)]
83. Houser, J.; Clement, J.; Pezeshki, A.; Mench, M.M. Influence of architecture and material properties on vanadium redox flow battery performance. *J. Power Sources* **2016**, *302*, 369–377. [[CrossRef](#)]
84. Kumar, S.; Jayanti, S. Effect of flow field on the performance of an all-vanadium redox flow battery. *J. Power Sources* **2016**, *307*, 782–787. [[CrossRef](#)]
85. Messaggi, M.; Canzi, P.; Mereu, R.; Baricci, A.; Inzoli, F.; Casalegno, A.; Zago, M. Analysis of flow field design on vanadium redox flow battery performance: Development of 3D computational fluid dynamic model and experimental validation. *Appl. Energy* **2018**, *228*, 1057–1070. [[CrossRef](#)]
86. Aramendia, I.; Fernandez-Gamiz, U.; Martinez-San-Vicente, A.; Zulueta, E.; Lopez-Guede, J.M. Vanadium Redox Flow Batteries: A Review Oriented to Fluid-Dynamic Optimization. *Energies* **2021**, *14*, 176. [[CrossRef](#)]
87. Huang, Z.; Mu, A.; Wu, L.; Wang, H. Vanadium redox flow batteries: Flow field design and flow rate optimization. *J. Energy Storage* **2022**, *45*, 103526. [[CrossRef](#)]
88. Prumbohm, E.; Becker, M.; Flaischlen, S.; Wehlinger, G.D.; Turek, T. Flow field designs developed by comprehensive CFD model decrease system costs of vanadium redox-flow batteries. *J. Flow Chem.* **2021**, *11*, 461–481. [[CrossRef](#)]
89. Jyothi Latha, T.; Jayanti, S. Ex-situ experimental studies on serpentine flow field design for redox flow battery systems. *J. Power Sources* **2014**, *248*, 140–146. [[CrossRef](#)]
90. He, Q.; Yu, J.; Guo, Z.; Sun, J.; Zhao, S.; Zhao, T.; Ni, M. Modeling of vanadium redox flow battery and electrode optimization with different flow fields. *e-Prime Adv. Electr. Eng. Electron. Energy* **2021**, *1*, 100001. [[CrossRef](#)]
91. Gundlapalli, R.; Kumar, S.; Jayanti, S. Stack Design Considerations for Vanadium Redox Flow Battery. *INAE Lett.* **2018**, *3*, 149–157. [[CrossRef](#)]
92. Sujali, S.; Mohamed, M.R.; Oumer, A.N.; Ahmad, A.; Leung, P. Study on architecture design of electroactive sites on Vanadium Redox Flow Battery (V-RFB). *E3S Web Conf.* **2019**, *80*, 02004. [[CrossRef](#)]
93. Ghimire, P.C.; Bhattarai, A.; Schweiss, R.; Scherer, G.G.; Wai, N.; Yan, Q. A comprehensive study of electrode compression effects in all vanadium redox flow batteries including locally resolved measurements. *Appl. Energy* **2018**, *230*, 974–982. [[CrossRef](#)]
94. He, H.; Tian, S.; Tarroja, B.; Ogunseitan, O.A.; Samuelsen, S.; Schoenung, J.M. Flow battery production: Materials selection and environmental impact. *J. Clean. Prod.* **2020**, *269*, 121740. [[CrossRef](#)]

Disclaimer/Publisher's Note: The statements, opinions and data contained in all publications are solely those of the individual author(s) and contributor(s) and not of MDPI and/or the editor(s). MDPI and/or the editor(s) disclaim responsibility for any injury to people or property resulting from any ideas, methods, instructions or products referred to in the content.